



**HAL**  
open science

# TiO<sub>2</sub> nanoparticle dispersions in water and nonaqueous solvents studied by gravitational sedimentation analysis: Complementarity of Hansen Parameters and DLVO interpretations

Lucie Delforce, Véronique Rataj, Véronique Rataj, Jean-Marie Aubry

## ► To cite this version:

Lucie Delforce, Véronique Rataj, Véronique Rataj, Jean-Marie Aubry. TiO<sub>2</sub> nanoparticle dispersions in water and nonaqueous solvents studied by gravitational sedimentation analysis: Complementarity of Hansen Parameters and DLVO interpretations. *Colloids and Surfaces A: Physicochemical and Engineering Aspects*, 2021, *Colloids and Surfaces A. Physicochemical and Engineering Aspects*, 628, pp.127333. 10.1016/j.colsurfa.2021.127333 . hal-04309454

**HAL Id: hal-04309454**

**<https://hal.univ-lille.fr/hal-04309454v1>**

Submitted on 22 Jul 2024

**HAL** is a multi-disciplinary open access archive for the deposit and dissemination of scientific research documents, whether they are published or not. The documents may come from teaching and research institutions in France or abroad, or from public or private research centers.

L'archive ouverte pluridisciplinaire **HAL**, est destinée au dépôt et à la diffusion de documents scientifiques de niveau recherche, publiés ou non, émanant des établissements d'enseignement et de recherche français ou étrangers, des laboratoires publics ou privés.



Distributed under a Creative Commons Attribution - NonCommercial 4.0 International License

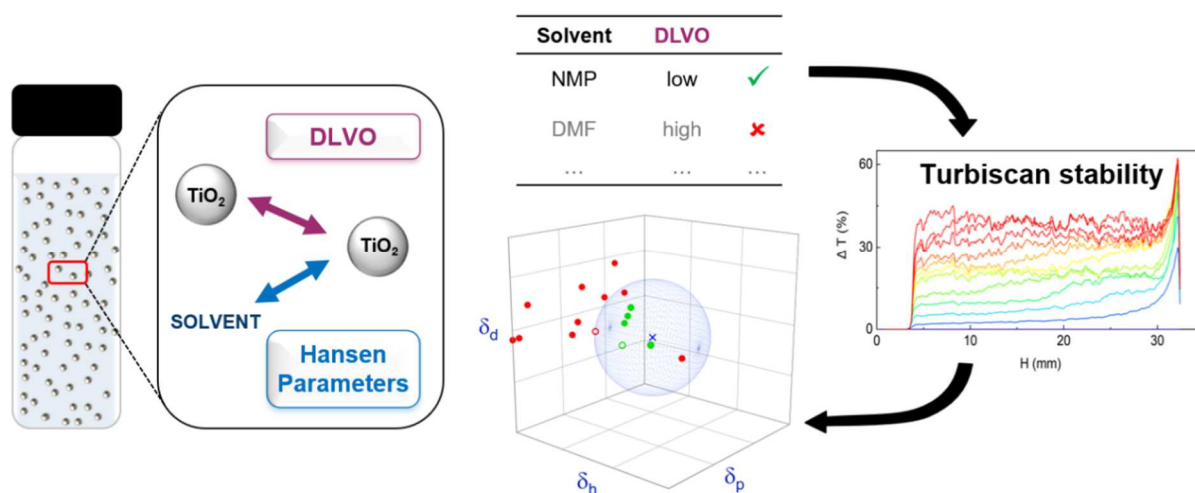
# TiO<sub>2</sub> nanoparticle dispersions in water and nonaqueous solvents studied by gravitational sedimentation analysis: Complementarity of Hansen Parameters and DLVO interpretations

Lucie Delforce<sup>1</sup>, Evamaria Hofmann<sup>2</sup>, Véronique Nardello-Rataj<sup>1\*</sup>, Jean-Marie Aubry<sup>1\*</sup>

<sup>1</sup> Univ. Lille, CNRS, Centrale Lille, Univ. Artois, UMR 8181 – UCCS – Unité de Catalyse et Chimie du Solide, F-59000 Lille, France.

<sup>2</sup> Univ. Regensburg, Institute of Theoretical and Physical Chemistry, 93053 Regensburg, Germany  
e-mail: jean-marie-aubry@univ-lille.fr and veronique.rataj-nardello@univ-lille.fr

## Abstract



Hansen Solubility Parameters (HSP) have been shown to be an effective approach for rationalizing and predicting the stability of titanium dioxide nanoparticles (TiO<sub>2</sub> NPs) dispersions. However, interparticle electrostatic interactions, not considered in Hansen's approach but taken into account in the DLVO theory, are expected to play a significant role in organic solvents having a notable dielectric constant.

Zeta potential  $\zeta$  of TiO<sub>2</sub> P25 NPs was measured in both aqueous and organic media to identify DLVO-stabilized dispersions from those stabilized by more specific NP-solvent interaction. Stability was quantified using a Turbiscan optical device which provides Stokes diameters and Relative Turbiscan Stability Index (RTSI).

When the zeta potential of NPs and the dielectric constant of the solvent are both high, the dispersion benefits from additional stabilization while when the electrostatic repulsion is negligible, only the solvents within a Hansen dispersion sphere give stable dispersions. The two interpretations are therefore complementary to describe the behavior of TiO<sub>2</sub> dispersions in organic solvents.

**Keywords:** dispersion; titanium dioxide; nonaqueous solvents; DLVO; Hansen Parameters; Turbiscan

## 1. Introduction

Nanoscience occupies an important place in research and industry. Due to their size less than 100 nm [1], nanoparticles (NPs) have peculiar properties relevant for applications in coatings, cosmetics, pharmaceuticals, energy and agriculture, to name a few [2,3]. Titanium dioxide nanoparticles ( $\text{TiO}_2$  NPs) are among the most widely used NPs, in particular as UV filters in sunscreen cosmetics [4] and plastics to avoid solar degradation [5], but also as photocatalysts in wastewater treatment [6], in self-cleaning transparent coatings [7], in solar cells or as silicon heat-stabilizers [8] and many other applications that require their dispersion in fluid or solid matrixes. It is of major importance that NPs be and remain homogeneously dispersed in the matrix to achieve optimal properties and stability. For instance, the efficiency of UV filters for skin protection is highly dependent on the distribution of this filter in the sunscreen film [9]. When  $\text{TiO}_2$  NPs are used as catalysts for wastewater treatment, photocatalytic degradation of pollutants increases with NPs dispersion as it is necessary that a large fraction of the catalytic area is accessible [10]. Moreover, well dispersed nano-scaled particles allow the production of transparent materials [7].

Nanoparticle dispersions can be studied by various experimental methods such as DLS (Dynamic Light Scattering) for size measurement [11–13] as well as gravitational [14–17] or centrifugal [13,18,19] sedimentations coupled with multiple light scattering methods which can provide more detailed information regarding the destabilization mechanisms of dispersions. These techniques are based on the measurement of transmitted and backscattered light over time along the whole height of a cell containing the dispersion. Both methods allow to determine hydrodynamic radius using sedimentation rate. However, agglomeration and flocculation of NPs, due to interparticle attraction, are more efficiently observed by gravitational sedimentation. Actually, when a sample is centrifuged, sedimentation is greatly accelerated whereas attractive interactions remain identical to that under gravitational field and, therefore, do not have time to induce agglomeration of the particles.

In this work, we study the evolution over time of aqueous and organic liquid dispersions of uncoated  $\text{TiO}_2$  nanoparticles using an optical device. The experiments are carried out under gravitational field in order to observe both the agglomeration and flocculation phenomena that occur when formulations are stored under ordinary conditions. In aqueous media, interparticle interactions are well described by the DLVO theory, named after the researchers Derjaguin, Landau, Verwey and Overbeek. Electrostatic repulsions between charged particle

surfaces and van der Waals attractions coming from the solid core of particles contribute to the overall particle interactions [20] and become dominant over gravity as particles get smaller [21,22]. However, it is recognized in the literature that organic solvents behave in a more complex manner than water as NP dispersing media because of their diversity in structure and polarity.

#### Hansen Solubility Parameters (HSP)

approach derives from the Hildebrand solubility parameter which is the square root of cohesive energy density. Hansen's assumption is that this cohesive energy density is due to three types of interactions between molecules: polar ( $\delta_p$ ), dispersive ( $\delta_d$ ) and hydrogen bonding ( $\delta_h$ ) interactions [23]. Originally, Hansen's solubility parameters were developed to study and anticipate the solubilization of molecular and macromolecular compounds in organic solvents. Hansen himself proposed to apply his method to characterize the surface of dispersed particles by arguing that organic liquids which adsorb most strongly to the surfaces of particles are those in which dispersions are most stable [23,24]. It is also argued that for small nanoparticles, energy of solvation can be  $< 0$  kT [25] and thus, solvation would be thermodynamically favoured, placing NPs in the frame of Hansen Parameters [26]. However, as the physicochemical phenomena involved in the dispersion of particles are definitely different from those involved in the dissolution of organic compounds, Süß et al. proposed to use the term "Hansen's Dispersion Parameters" (HDP) instead of HSP when Hansen's approach is used to study the dispersibility and stability of particles [13]. HSP has been shown to be a versatile tool for rationalizing and predicting the stability of various types of NP dispersions such as carbon black [13], carbon nanofibers [27], fullerene [28], graphene [29] and carbon nanotubes [30] but also titanium carbides [31] and inorganic nanoparticles of ZnO, Al<sub>2</sub>O<sub>3</sub>, ZrO<sub>2</sub> [32], hydroxyapatite and TiO<sub>2</sub> [18]. In practice, the particles are dispersed in a series of carefully chosen solvents according to a standard protocol. Each solvent is assigned a score based on the stability of the dispersion, then a Hansen sphere including the most effective solvents is built in the 3D Hansen space. However, it can be expected that interparticle electrostatic interactions, not considered in Hansen's approach, also play a significant role, especially in organic solvents with notable dielectric constant. Many other solvent scales such as donor numbers (DN), solvatochromic Kamlet-Taft descriptors and Reichardt's E<sub>T</sub>(30) could be used to quantify solvent-particle interactions. This work is based on Hansen Parameters as the three complementary parameters allow a practical 3D representation and a clear visualization of effective and non-effective solvents.

Herein we discuss the respective contributions of DLVO and non-DLVO interactions in the stability of TiO<sub>2</sub> P25 nanoparticle dispersions, with a special emphasis on the relevance of the HSP concept to rationalize non-DLVO interactions in organic solvents. Zeta potential

measurements in organic and aqueous media are carried out to identify the solvents in which stability can be explained by the DLVO theory from those for which the stability results from more specific NP-solvent interaction. These latter solvents are used to determine the Hansen sphere of TiO<sub>2</sub> P25 with a Turbiscan as a stability analyser.

## 2. Experimental

### 2.1. Chemicals

The nanoparticles AEROXIDE® TiO<sub>2</sub> P25 (titanium dioxide, purity ≥ 99.5 %) were obtained from Acros Organics (Thermo Fisher Scientific Inc., Geel, Belgium). These uncoated TiO<sub>2</sub> nanoparticles (NPs) had a specific surface area of 35 – 65 m<sup>2</sup>/g [8] and an average primary particle diameter of 21 nm [33]. The crystal structure was mainly anatase (85 %) and rutile (15 %) [34].

Organic solvents used as dispersion media were supplied by the companies Sigma-Aldrich Chemie GmbH (St. Louis, USA), VWR International GmbH (Radnor, Pennsylvania), Acros Organics (Thermo Fisher Scientific Inc., Geel, Belgium), Alfa Aesar (Thermo Fisher Scientific Inc., Heysham, UK), Honeywell (Honeywell International Inc., Morristown, USA), Verbièse (Laboratoire Verbièse, Merville, France) and TCI (Tokyo Chemical Industry Co. Ltd., Tokyo, Japan). They were all of the highest purity available and used as such. Trifluoroacetic acid (99 %) was supplied by Alfa Aesar and tetrabutylammonium hydroxide (1 M in methanol) was supplied by Sigma-Aldrich. Ultrapure water was obtained using a Thermo Scientific Barnstead MicroPure Ultrapure water system with a resistivity of 18.2 MΩ.cm.

### 2.2. Protocol for dispersing TiO<sub>2</sub> P25 nanoparticles

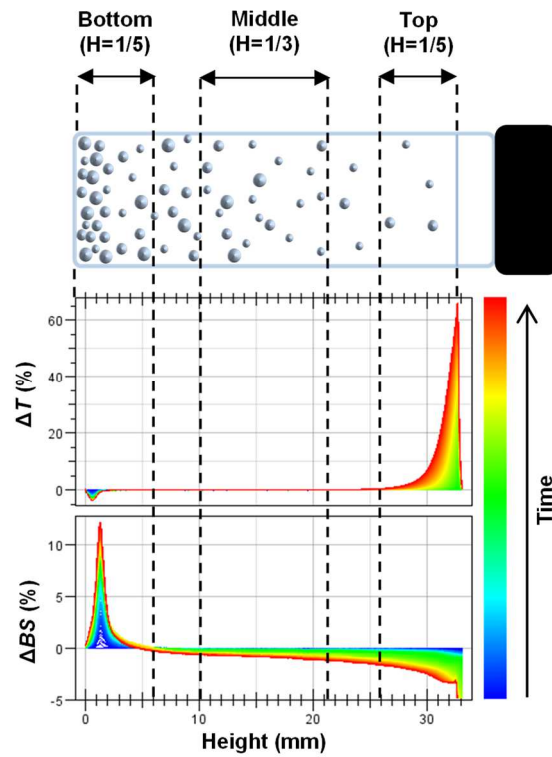
**Aqueous dispersions.** pH-controlled solutions were prepared by mixing NaCl 10<sup>-3</sup> M and either NaOH or HCl 10<sup>-3</sup> M solutions in order to maintain ionic strength at a constant value of 10<sup>-3</sup> M. 20 mg of TiO<sub>2</sub> was placed in a borosilicated glass cell (from Formulacion Company, 27.5 mm diameter), then 20 mL NaCl 10<sup>-3</sup> M and HCl or NaOH 10<sup>-3</sup> M were added. The cell was placed in a 23.0 °C thermoregulated bath and sonicated for 12 min using an ultrasonic probe Sonotrode S26d2 (2 mm diameter) immersed by 5 mm in the liquid and operated by the ultrasonic processor UP200St (both from Hielscher). The sonotrode pulse was fixed at 50 % and the amplitude at 20 %. Thermoregulation was carried out by means of a Huber Ministat 125 circulating water bath. pH was measured by immersing the electrode directly in the cell and a sample was taken to measure particle size and zeta-potential ζ using a Zetasizer Nano ZS from Malvern Panalytical. The cell was wiped to remove water drops from the outside wall and was scanned by a thermoregulated Turbiscan LAB from Formulacion.

**Dispersions in organic solvents.** In organic solvents, 20 mL of solvent (“pure” in the first

series of experiments and containing  $10^{-3}$  M trifluoroacetic acid or tetrabutylammonium hydroxide afterwards) were sampled with a graduated pipette and added to a borosilicated glass cell containing 20 mg of  $\text{TiO}_2$ . The particles were then dispersed and analysed according to the protocol described above.

### 2.3. Turbiscan measurement

Dispersions were scanned every 30 seconds for 2 to 72 hours at 25.0 °C. Measured signals are transmitted light ( $T$ ) and backscattered light ( $BS$ ) represented as a function of the sample height. Variations in  $T$  and  $BS$  can be seen by deducting the first scan to all the following scans yielding  $\Delta T$  and  $\Delta BS$ . Typical resulting spectra are shown in **Figure 1**.



**Figure 1** – Change of transmitted light ( $\Delta T$ ) and backscattered light ( $\Delta BS$ ) from Turbiscan data for a partially sedimented dispersion.  $T$  increases at the top and  $BS$  increases at the bottom as particles sediment over time.

Experimental data were processed using the TurbiSoft Lab software (2.3.1.125 FAnalyser) and  $TSI$  (Turbiscan Stability Index) was computed according to the following equation [35].

$$TSI(t) = \frac{1}{N_h} \sum_{t_i=1}^{t_{max}} \sum_{z_i=z_{min}}^{z_{max}} |BS, T(t_i, z_i) - BS, T(t_{i-1}, z_i)| \quad (1)$$

with  $t_{max}$  the measurement time at which the  $TSI$  is calculated,  $z_{min}$  and  $z_{max}$  the lower and

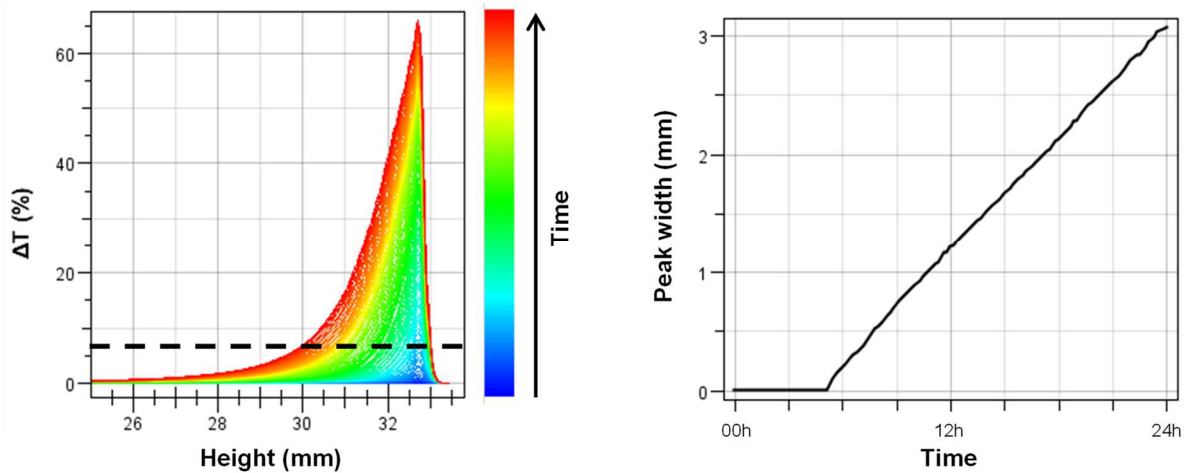
upper selected height limits respectively,  $N_h = (z_{max} - z_{min})/\Delta h$  the number of height positions in the selected zone of the scan and  $BS, T$  the considered signal (backscattering  $BS$  if  $T < 0.2\%$  or transmission  $T$  otherwise). Consequently,  $TSI = 0$  for  $t = 0$  and increases as the sample gets destabilized. High  $TSI$  values are characteristic of unstable dispersions. In organic media, a Relative Turbiscan Stability Index ( $RTSI$ ) was defined according to equation (2) to compare solvents with each other, so as to consider their viscosity  $\eta$  [cP] and their density  $\rho_i$  [g.cm<sup>-3</sup>] which modify the sedimentation rate according to Stokes' law.

$$RTSI = TSI \times \frac{\eta}{(\rho_{particle} - \rho_{solvent})} \quad (2)$$

Moreover, the variations of  $T$  (or  $BS$  when the sample is opaque) allow the calculation of mean particle size *via* Stokes sedimentation. Using the width evolution at a threshold of the  $\Delta T$  clarification peak at the top of the cell (see **Figure 2**), the migration rate of particles corrected by the viscosity and density of the solvent is linked to particle size by equation (3) [36]. A threshold of  $\Delta T = \Delta T_{max}/10$  was chosen to measure  $d_{Stokes}$  in all samples. When variation of the peak width was not linear, due to sedimentation of different size populations in the sample, the initial slope was used. A comparison with DLS size measurement was made for TiO<sub>2</sub> P25 dispersions in non-aqueous solvents and is available in SI. In the case of non-monomodal population, significant differences between  $d_{DLS}$  and  $d_{Stokes}$  occur. In this work, we chose to consider  $d_{Stokes}$  to evaluate particle size.

$$v = \frac{d^2 \times g \times (\rho_p - \rho_f)}{18 \eta} \times \frac{1 - \phi}{1 + \frac{4.6 \phi}{(1 - \phi)^3}} \quad (3)$$

with  $v$  the sedimentation rate,  $\phi$  the solid volume fraction,  $d$  the diameter,  $g$  the gravitational constant,  $\rho_p$  and  $\rho_f$  the density of particles and fluid respectively and  $\eta$  the viscosity.



**Figure 2** -  $\Delta T$  clarification peak and threshold at  $\Delta T = \Delta T_{max}/10$  (left). Peak width evolution at the 1/10 threshold (right) : the slope corresponds to the sedimentation rate  $v$ .

## 2.4. Zeta potential measurement

Immediately after dispersing the NPs, 1 mL of dispersion was introduced in a folded capillary zeta cell (aqueous dispersions) or a dip cell (dispersions in organic solvents) and the zeta potential of TiO<sub>2</sub> suspensions was measured using a Zetasizer Nano ZS from Malvern Panalytical. In organic solvents, measuring  $\zeta$  is more challenging than in water. Indeed, the usual folded capillary cell made out of polycarbonate cannot be used for two reasons. Firstly, capillary zeta cells are made of polycarbonate that can be dissolved by some organic solvents. Being made of polyether-ether-ketone (PEEK) polymer and a glass cuvette with excellent chemical compatibility, the dip cell is more addressed for this type of measurements. Secondly, low conductivity media require a higher applied field to observe electrophoretic mobility. The dip cell electrodes are positioned closely together on the PEEK probe, producing greater electric fields with lower voltage and thus avoiding local heating and electrolysis effects [37,38].

Zeta potential is the potential at the surface between a rigidly adsorbed layer and the freely flowing solvent molecules [39]. The functional groups at the particle surface interact with the dispersing medium. Dipole-dipole interactions induce the creation of electric charges that affect the electrostatic forces of particles with one-another. The measurement is based on laser Doppler electrophoresis. The zetasizer measures the frequency difference between the incident and the backscattered beams on the chamber detectors. This Doppler effect is induced by the particle movement under the difference of electric potential. Zeta potential  $\zeta$  is then calculated using Hückel's equation [40]:

$$u_{Hückel} = \frac{2 \varepsilon_0 \varepsilon_r \zeta}{3 \eta} \quad (4)$$

with  $u$  the particle mobility,  $\varepsilon_r$  the relative permittivity of the solvent,  $\varepsilon_0$  the electrical permittivity of vacuum and  $\eta$  the viscosity.

Three concordant zeta measurements were achieved for each sample, and values reported in this work are the average zeta values. Uncertainty of measurement is estimated to be the standard deviation. In organic solvents, zeta deviation is generally larger than in aqueous media. Zeta potentials measured in solvents without the addition of electrolytes should be considered specific to this study as it may differ according to experimental conditions, namely the solvent purity, supplier or batch. Zeta potential of TiO<sub>2</sub> in nonaqueous solvents is very sensitive to the presence and nature of impurities [41,42].



## 2.5. Hansen sphere calculation

Two HSP spheres of TiO<sub>2</sub> P25 were determined based on either one of two distinct stability criteria, namely  $d_{\text{Stokes}}$  and RTSI. Solvents were rated according to one of these parameters: score 1 for “good” dispersing media (stable dispersion) and score 2 for “bad” dispersing media (unstable dispersion). A threshold was defined for  $d_{\text{Stokes}}$  and RTSI as follows.

Score 1:  $d_{\text{Stokes}} < 0.31 \mu\text{m}$  or  $RTSI_{2h}^{\text{top}} < 1.0$

Score 2:  $d_{\text{Stokes}} > 0.31 \mu\text{m}$  or  $RTSI_{2h}^{\text{top}} > 1.0$

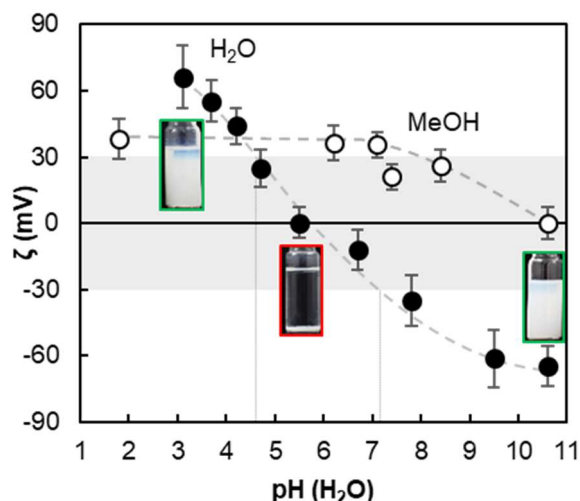
Using HSPiP software and the scores attributed to each solvent, the spheres are computed so as to include scores 1 and exclude scores 2. The fit indicator reflects the quality of the sphere computation: it decreases if scores 1 are excluded and scores 2 are included in the sphere. The center of the sphere, represented by the three coordinates  $\delta_d$ ,  $\delta_p$  and  $\delta_h$ , corresponds to the Hansen Solubility Parameters of TiO<sub>2</sub>.

## 3. Results and discussion

The stability of TiO<sub>2</sub> nanoparticle dispersions was studied in various aqueous and organic liquid media and at different pH by gravitational sedimentation analysis using the optical analyser Turbiscan. Two complementary approaches were used to analyse and interpret the results. The first, based on DLVO theory, is well suited to dispersions in water and in highly polar organic solvents in which electrostatic repulsions play a major role, while the second, based on Hansen's solubility parameters, makes account for non-DLVO interactions in organic solvents when repulsive electrostatic interactions are weak.

### 3.1. Aqueous TiO<sub>2</sub> dispersions

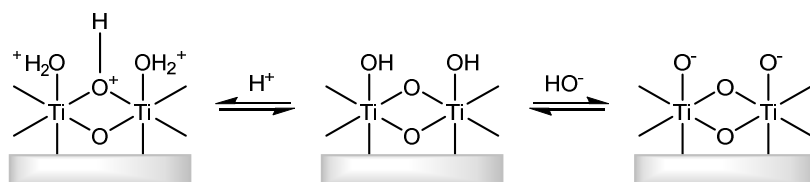
Zeta potential  $\zeta$  is the key parameter to rationalize the stability of aqueous TiO<sub>2</sub> dispersions [11,43–45]. **Figure 3** (filled dots ●) shows the evolution of  $\zeta$  as a function of pH in aqueous solution at constant ionic strength.



**Figure 3** - Evolution of 1 g/L TiO<sub>2</sub> P25 nanoparticle zeta potential with pH in water (●) and methanol (○) at 25.0 °C referred to the aqueous pH scale. pH is adjusted with HCl and NaOH. Ionic strength is kept constant at 10<sup>-3</sup> M with NaCl. Instability area is marked in grey, corresponding to pH 4.6 to 7.2 in water. Pictures of dispersions in water at pH 3.1, 5.5 and 10.6 (left to right) are taken after 24 hours.

When dispersed in solution, NPs collide with each other due to the Brownian movement. They can either agglomerate or rebound depending on the relative strength of the van der Waals attraction and the electrostatic repulsion. The DLVO theory which quantitatively accounts for these two types of interactions, was initially developed to rationalize the stability of dispersions in aqueous media [46,47].

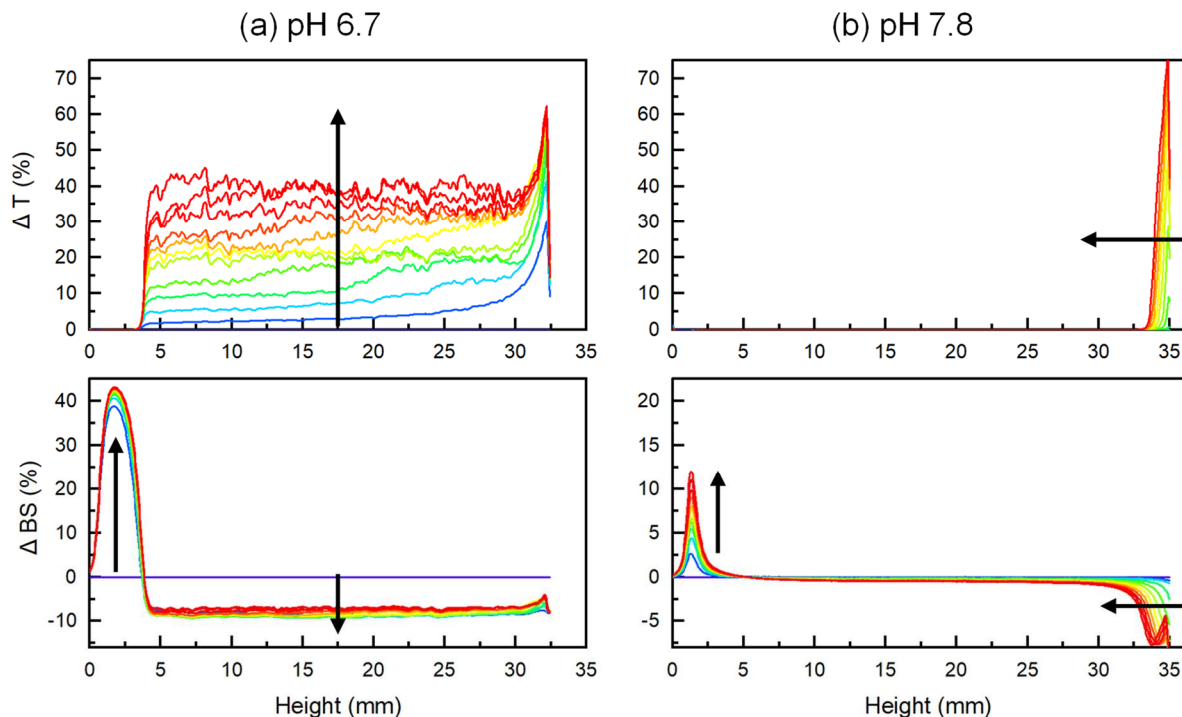
Surface charge effects of TiO<sub>2</sub> dispersions in water have been extensively studied [11,43–45,48,49]. The pH of the aqueous solution plays an important role as it influences ion exchanges between NPs and water, modifying the surface charge and accordingly, the zeta potential. Indeed, the presence of acidic Ti<sup>IV</sup> sites on the surface causes water dissociation by adsorption, creating -OH functional groups [48]. NP surface is then modified *via* reaction with H<sup>+</sup> or HO<sup>-</sup> ions according to equilibria as depicted in **Figure 4** [48,50].



**Figure 4** – Simplified illustration of electric charges formation on TiO<sub>2</sub> surface by acido-basic reactions in water.

Bidentate bridge OH between two Ti atoms (Ti-OH<sup>+</sup>-Ti) and monodentate terminal H<sub>2</sub>O adsorbed on 5-fold Ti sites have pK<sub>a</sub> values of 2.9 and 12.7 respectively [51]. The reported

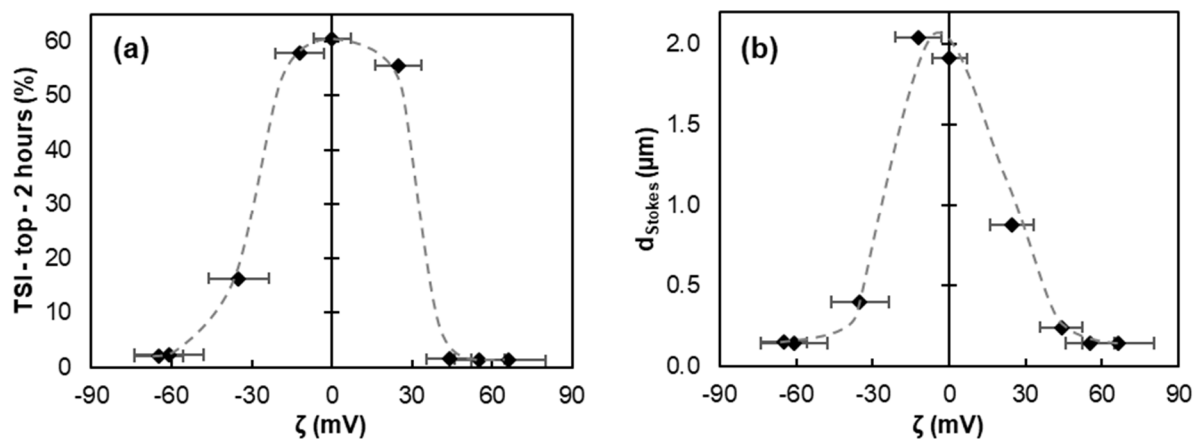
values for the isoelectric point of TiO<sub>2</sub> P25 are comprised between 5.8 and 6.6 [48,51–53]. As shown in **Figure 3 (●)**, an isoelectric point of 5.9 was found in accordance with the literature data. Electrolyte concentration is also known to strongly impact the zeta potential as more counter-ions can screen surface charges when its concentration increases. Those differences between measured zeta potential and surface potential are minimized at low electrolyte concentration and with monovalent ions [46,47,54]. In this work, pH was adjusted by NaOH or HCl addition and the ionic strength was then adjusted to a constant value of 10<sup>-3</sup> M by NaCl addition. pH ranging from 4.6 to 7.2 causes  $\zeta$  to be comprised within the -30 mV to 30 mV interval (**Figure 3 ●**) leading to quickly destabilized dispersions. Such destabilizations can be finely analysed using a Turbiscan through the detection of the transmission  $T$  and backscattered  $BS$  light signals. Indeed, using  $T$  and  $BS$  signals, the average  $TSI$  value (eq. 1) can be calculated on any portion of the cell and at any time of the analysis (see experimental section). It is worth noting that phenomena differ depending on the height: at the top,  $T$  increases faster than below as clarification occurs. **Figure 5** shows the evolution of the transmitted  $T$  and backscattered  $BS$  lights of two aqueous TiO<sub>2</sub> nanoparticle dispersions at pH 6.7 and pH 7.8.



**Figure 5** - Variations over 2 hours of transmitted  $T$  and backscattered  $BS$  light of aqueous TiO<sub>2</sub> P25 1 g/L dispersions ( $T = 25.0$  °C) at pH 6.7 and  $\zeta = -8$  mV (a) and at pH 7.8 and  $\zeta = -23$  mV (b).

When DLVO repulsion is strong enough to avoid particle agglomeration, the typical profile is

the one in **Figure 5b**.  $T$  signal shows no variation except at the top, where slow sedimentation occurs. With time, the sedimentation front (also visible in  $BS$  light) would eventually reach the bottom of the cell.  $BS$  light increases as particles accumulate at the bottom. Those samples are easily re-dispersed with a simple re-agitation. On the contrary, when DLVO repulsion is weak (i.e., zeta potential is less than 30 mV), as in **Figure 5a**, destabilization is fast.  $BS$  decreases and  $T$  increases at the top and in the middle of the cell due to particle agglomeration. Indeed, the particle concentration decreases as they agglomerate.  $T$  even turns into an irregular signal when agglomerates tend to be individually distinguishable. Sedimented particles accumulate faster if DLVO repulsion is low: the increasing size of agglomerates, in turn, accelerates their sedimentation rate. All those variations over time can be accounted for by the  $TSI$  value.  $TSI$  represented in **Figure 6a** has been calculated at the top of the cell in order to detect the very early changes even for the most stable samples. After 2 hours,  $TSI_{2h}^{top}$  values match the expected dispersions behaviour in accordance with the DLVO theory. When  $|\zeta| < 20$  mV,  $TSI_{2h}^{top}$  is significantly higher than outside these boundaries. Destabilization is faster within this interval whereas solutions with high  $|\zeta|$  remain stable. In **Figure 6b**, the Stokes diameters have been reported as a function of  $\zeta$ . They reach a maximum around the isoelectric point and are noticeably smaller as  $|\zeta|$  increases. All these findings clearly show that Turbiscan  $TSI_{2h}^{top}$  and Stokes diameters appear as reliable values to quantify dispersion stability. In particular, the maximum  $d_{Stokes}$  being attained for zeta potentials close to 0 mV is in accordance with the increase of coagulation rate when electrostatic repulsion is low. In that case, there exists little or no energetic barrier to prevent particles from colliding and coagulation occurs rapidly [55].



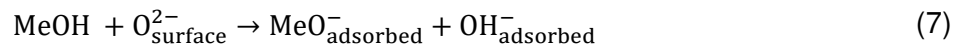
**Figure 6** – Evolution at 25.0 °C of (a)  $TSI$  at the top of the cell after 2 hours and (b) Stokes diameters determined using the Turbiscan with zeta potential  $\zeta$  of 1 g/L  $TiO_2$  P25 aqueous dispersions. Ionic strength is kept constant at  $10^{-3}$  M by NaCl addition, pH is adjusted using NaOH and HCl solutions.

### 3.2. TiO<sub>2</sub> dispersions in methanol and other nonaqueous solvents

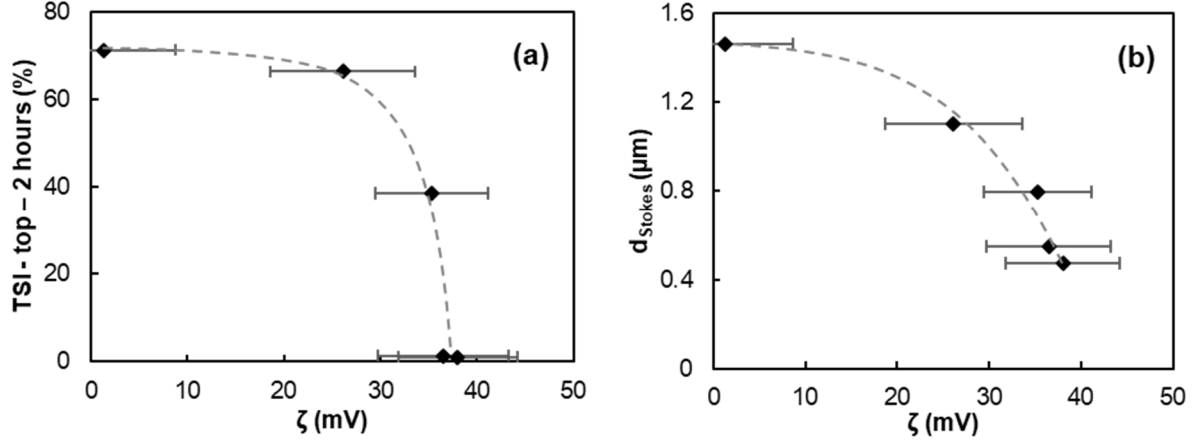
DLVO theory was initially developed to quantitatively account for interactions between particles in aqueous media but it can also be applied to organic dispersing media [15,56,57]. The main differences between aqueous and organic dispersing media concern dielectric constants and electrolyte concentrations. Both those factors impact the electrostatic repulsion potential.

The stability of TiO<sub>2</sub> dispersion was investigated in a common polar and protic solvent, namely methanol. **Figure 3** (empty dots O) shows the variation of the zeta potential at different pH values measured using a glass electrode standardized in aqueous buffer. The pH range accessible, based on the water scale, is -1.8 to 17.2 and depends on the dissociation constants of methanol [58]. The lower limit is given by the transfer activity coefficient of H<sup>+</sup> ions in methanol  $p\gamma_{H_2O \rightarrow MeOH}^t(H^+) = -1.8$  and the upper limit is given by the autoprotolysis constant of methanol  $pK_{MeOH} = 17.2$  [58–60].

First of all, in contrast to aqueous media, it appears that whatever the pH value,  $\zeta$  remains positive. A quite similar observation was made by Kosmulski et al. for TiO<sub>2</sub> in water/methanol mixtures: zeta potential became closer to 0 mV with increasing amounts of methanol [61]. On the other hand, it slightly increases with the addition of HCl, whereas NaOH addition brings  $\zeta$  closer to 0 mV but not in the negative values. Dissociative adsorption of methanol on a hydrated TiO<sub>2</sub> surface is described by the following equations [62].



As a result, surface hydroxyl groups (shown in Figure 4) are partially replaced by methoxyl groups, which are not able to donate protons. The creation of negative surface charges in the presence of NaOH is thus reduced. Moreover, in the presence of electrolytes, there exists a charge screening from Na<sup>+</sup> and Cl<sup>-</sup> ions. It is assumed that Cl<sup>-</sup> ions interact with the surface through TiOH<sub>2</sub><sup>+</sup>Cl<sup>-</sup> interactions, whereas Na<sup>+</sup> ions interact in a non-specific way with negatively charged groups on TiO<sub>2</sub> surface [62]. When NaOH is added to methanol dispersions, TiOH<sub>2</sub><sup>+</sup> disappears from the surface and Cl<sup>-</sup> ion adsorption decreases while Na<sup>+</sup> ion adsorption ability remains identical. This may explain why the zeta potential remains positive whereas surface potential may be negative. **Figure 7** displays the evolution of  $TSI_{2h}^{top}$  and Stokes diameters determined with the Turbiscan as a function of the zeta potential  $\zeta$  in methanol.



**Figure 7** - Evolution of (a) TSI at the top of the cell after 2 hours and (b) Stokes diameters  $d_{\text{Stokes}}$  as a function of the zeta potential of 1 g/L TiO<sub>2</sub> P25 particles in methanol. Ionic strength is kept constant at  $10^{-3}$  M with NaCl and pH is adjusted with NaOH or HCl.

As in water,  $TSI_{2h}^{\text{top}}$  and particle diameters vary depending on the zeta potential suggesting heavily that the stability of TiO<sub>2</sub> dispersions in methanol is mainly influenced by electrostatic repulsions as in water. Actually, it is well established that DLVO theory is also applicable in polar organic solvents and may explain the stability of dispersions provided that the dielectric constant is high enough. However, for solvents of lower permittivity  $\varepsilon$ , electrostatic repulsions significantly decrease even when zeta potential is relatively high. Indeed, the repulsion potential  $V_R$  between two spheres is given by the following expression [63].

$$V_R = 2 \pi \varepsilon a \zeta^2 \log(1 + \exp(-R\kappa)) \quad (8)$$

where  $\varepsilon$  is the solvent permittivity,  $a$  is the particle radius,  $\zeta$  is the zeta potential,  $R$  is the distance between two spheres and  $\kappa^{-1}$  the the Debye-Hückel distance defined by [64].

$$\kappa^{-1} = \sqrt{\frac{\varepsilon k_B T}{2 N_A e^2 I}} \quad (9)$$

where  $k_B$  is the Boltzmann constant,  $N_A$  is the Avogadro constant,  $e$  is the electron charge and  $I$  is the ionic strength. The attractive component  $V_A$ , described by Hamaker [65], is given by equation (10).

$$V_A = \frac{-A_{12} a}{12 R} \quad (10)$$

Hamaker's constant  $A_{12}$  of component 2 in medium 1 is calculated with Eq. (11) from each component constants  $A_1$  and  $A_2$  expressed by Eq. (12) [21].

$$A_{12} = (\sqrt{A_1} - \sqrt{A_2})^2 \quad (11)$$

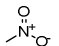
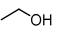
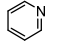
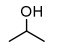
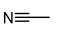
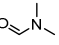
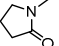
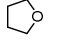
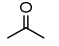
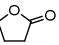
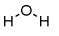
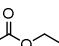
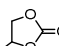
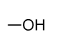
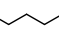
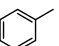
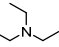
$$A_i = \frac{3}{4} k_B T \frac{(\varepsilon_{r,i} - 1)^2}{(\varepsilon_{r,i} + 1)^2} + \frac{3h\nu_e(n_i^2 - 1)^2}{16\sqrt{2}(n_i^2 + 1)^{3/2}} \quad (12)$$

$\varepsilon_r$  is the relative permittivity,  $h$  is Planck's constant,  $\nu_e$  is the main electronic absorption frequency for the dielectric permittivity (calculated based on ionization energies, details are given in SI) and  $n$  is the refractive index.

When the total interaction energy ( $V_R - V_A$ ) is below zero no energy barrier is opposed to the coagulation and the dispersion is extremely unstable. On the contrary, when ( $V_R - V_A$ ) is above  $25 k_B T$ , the electrostatic repulsion is so predominant over the Van der Waals attraction that the dispersion is kinetically stable although the thermodynamically stable state corresponds to particles in contact for lyophobic colloids [66]. Between these extreme cases, the energy barrier more or less stabilizes the dispersions without completely preventing aggregation.

According to formulas (8) and (9), the electrostatic repulsion between two particles depends mainly on the dielectric constant of the medium and the zeta potential of the particles. These two parameters were therefore considered for assessing the DLVO contribution to the stability of the dispersions. Zeta potential  $\zeta$  was measured in samples containing 1 g/L TiO<sub>2</sub> P25 nanoparticles dispersed in a series of 17 "pure" solvents, i.e., of the highest purity commercially available and free of any additional compound. The analysis of the transmitted and backscattered signals recorded by the Turbiscan for two hours provides the average diameter of the aggregates ( $d_{\text{Stokes}}$ ) as well as the so-called Relative Turbiscan Stability Index ( $RTSI_{2h}^{top}$ ). This corrected index is calculated from the  $TSI$  by taking into account the viscosity and density of the solvents (Eq. 2). The solvents are listed in Table 1 according to the increasing size of the aggregates.

Table 1 - Stability results and physicochemical characteristics of TiO<sub>2</sub> dispersions (1 g/L) in various “pure” solvents at 25 °C: viscosity ( $\eta$ ), density ( $\rho$ ), dielectric constant ( $\epsilon_r$ ), zeta potential ( $\zeta$ ), Relative Turbiscan Stability Index (RTSI), Stokes diameters ( $d_{\text{Stokes}}$ ) and total interaction energy  $(V_R - V_A)_{\text{max}}$  calculated according to equations (8-12). Calculation details are given in SI.

| Solvent                 | Structure   | $\eta$<br>(cP) | $\rho$<br>(g/cm <sup>3</sup> ) | $\epsilon_r$ | $\zeta$<br>(mV) | RTSI <sub>2h</sub> <sup>top</sup> | $d_{\text{Stokes}}$<br>( $\mu\text{m}$ ) | $\frac{(V_R - V_A)_{\text{max}}}{k_B T}$ |
|-------------------------|---|----------------|--------------------------------|--------------|-----------------|-----------------------------------|--|--|
| Nitromethane            |    | 0.67           | 1.13                           | 39.0         | 31 $\pm$ 9      | 0.3                               | 0.13                                     | 2.1                                      |
| Ethanol                 |    | 1.22           | 0.82                           | 24.5         | 31 $\pm$ 1      | 0.4                               | 0.14                                     | 1.1                                      |
| Pyridine                |    | 0.88           | 0.98                           | 12.4         | 44 $\pm$ 10     | 0.2                               | 0.18                                     | 0.9                                      |
| Isopropanol             |    | 2.1            | 0.79                           | 17.9         | -70 $\pm$ 9     | 0.8                               | 0.19                                     | 5.8                                      |
| Acetonitrile            |    | 0.37           | 0.79                           | 37.5         | -34 $\pm$ 10    | 0.9                               | 0.21                                     | 2.5                                      |
| DMF                     |    | 0.92           | 0.94                           | 36.7         | 43 $\pm$ 14     | 0.8                               | 0.26                                     | 4.6                                      |
| -----                   |   |                |                                |              |                 |                                   |  |  |
| NMP                     |  | 1.67           | 1.03                           | 33.0         | -7 $\pm$ 5      | 0.3                               | 0.40                                     | < 0                                      |
| THF                     |  | 0.95           | 0.98                           | 7.6          | 19 $\pm$ 2      | 1.4                               | 0.53                                     | < 0                                      |
| Acetone                 |  | 0.32           | 0.79                           | 20.7         | -26 $\pm$ 2     | 7.2                               | 0.81                                     | 0.2                                      |
| -----                   |   |                |                                |              |                 |                                   |  |  |
| $\gamma$ -Butyrolactone |  | 1.75           | 1.13                           | 41.0         | -4 $\pm$ 2      | 13.1                              | 0.89                                     | < 0                                      |
| Water                   |  | 0.89           | 1.00                           | 80.1         | -5 $\pm$ 4      | 14.5                              | 1.11                                     | < 0                                      |
| Ethyl Acetate           |  | 0.46           | 0.9                            | 6.0          | 44 $\pm$ 12     | 2.2                               | 1.14                                     | < 0                                      |
| Propylene Carbonate     |  | 2.8            | 1.2                            | 64.9         | -46 $\pm$ 6     | 28.4                              | 1.34                                     | 11.0                                     |
| Methanol                |  | 0.54           | 0.79                           | 32.7         | 11 $\pm$ 13     | 10.8                              | 2.88                                     | < 0                                      |
| Heptane                 |  | 0.42           | 0.68                           | 1.9          | -10 $\pm$ 3     | 5.6                               | 8.05                                     | < 0                                      |
| Toluene                 |  | 0.55           | 0.89                           | 2.4          | -30 $\pm$ 8     | 9.7                               | 9.47                                     | < 0                                      |
| Triethylamine           |  | 0.36           | 0.73                           | 2.4          | 6 $\pm$ 6       | 4.8                               | 9.59                                     | < 0                                      |

Most of the observed stabilities can be rationalized by the DLVO theory. It thus appears that the six solvents leading to the finest particles ( $d_{\text{Stokes}} < 0.3 \mu\text{m}$ ), namely nitromethane, ethanol, pyridine, isopropanol, acetonitrile and dimethylformamide, correspond to particles with a high zeta potential ( $|\zeta| > 30 \text{ mV}$ ) dispersed in quite polar solvents ( $\epsilon_r > 10$ ). On the



contrary, the seven solvents in which the aggregates are the largest ( $0.9 < d_{\text{Stokes}} < 10 \mu\text{m}$ ) have either a very low dielectric constant ( $\epsilon_r < 10$ ), namely ethyl acetate, heptane, toluene and triethylamine, or a low zeta potential ( $|\zeta| < 6 \text{ mV}$ ) insufficient for the electrostatic repulsion to dominate the Van der Waals attraction, namely,  $\gamma$ -butyrolactone, water and methanol. Three solvents (N-methyl pyrrolidone, tetrahydrofuran and acetone) have an intermediate behavior because either their dielectric constant or the zeta potential of the particles is slightly lower than the threshold values defined above.

Likewise, the evolution  $RTSI_{2h}^{\text{top}}$  (Table 1) follows the same trend as the best solvents exhibit low values ( $RTSI_{2h}^{\text{top}} < 1$ ) whereas the less efficient solvents have very high values ( $RTSI_{2h}^{\text{top}} > 10$ ). However, two solvents fail to fall into this general framework of explanation: N-methyl pyrrolidine (NMP) in which the dispersion is stable although the electrostatic repulsion is negligible ( $|\zeta| = 2.3 \text{ mV}$ ), and propylene carbonate which meets both stability criteria ( $\epsilon_r = 64.9$  and  $|\zeta| = 51.8 \text{ mV}$ ) but in which the dispersion is extremely unstable. The presence of these outliers indicates that other phenomena not considered in the DLVO theory are involved in the stability of  $\text{TiO}_2$  dispersions. To analyze the influence of non-DLVO forces, the alternative approach of Hansen's solubility parameters (HSP) is investigated below.

### 3.3. Stability of $\text{TiO}_2$ dispersions in organic solvents interpreted by Hansen's approach

The Hansen Solubility Parameters (HSP) method is a pragmatic and versatile tool originally developed to facilitate the finding of solvents able to dissolve paint resins. The principle of the method is based on the idea that "like dissolves like", which means that a solvent should effectively dissolve a solute provided it resembles it. This concept was quickly extended to solid/liquid dispersions to help formulators in designing the most suitable media for dispersing pigments. This variant is based on the "like disperses like" principle assuming that particles disperse better in solvents having high affinity for the surface.

In the HSP approach, only three types of interaction between the particle and the surrounding medium are considered, namely hydrogen bonding, dipolar interactions and dispersive interactions due to London forces. The attractive interactions of Van der Waals are considered in both theories HSP and DLVO. On the other hand, electrostatic repulsions are only considered in DLVO theory while hydrogen and dipole bonds are only considered in Hansen's approach. The decisive impact of electrostatic stabilization is clearly established in the case of charged  $\text{TiO}_2$  particles dispersed in polar solvents, but it is unable to explain the stability observed for some  $\text{TiO}_2$  dispersions when  $|\zeta|$  is low.

The estimation of the respective contributions of these complementary interactions would provide valuable information to rationalize the experimental results usually interpreted on the basis of only one of these theories. The difficulty to quantify the stability of a dispersion has been brought up in the literature and Süß et al. [13] proposed to use analytical centrifugation and quantify the sedimentation rate. This technique allows analyzing a large number of samples in a timely manner compared to gravitational sedimentation, but interparticle attraction and coagulation cannot be detected by this technique. In this work, we have chosen to use the Turbiscan device based on gravitational sedimentation which detects the two phenomena involved in the destabilization of dispersions under ordinary storage conditions. Namely, on the one hand, the coagulation of particles resulting from Brownian motion and Van der Waals attraction and, on the other hand, the sedimentation of particles and aggregates under the effect of gravity.

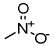
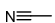
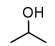
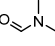
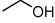
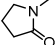
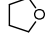
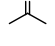
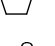
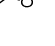



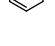
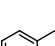
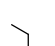
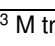
To focus on the influence of non-DLVO forces, the contribution of electrostatic repulsion to stabilization was minimized by decreasing the zeta potential of particles and removing the energy barrier. Thus, whenever  $(V_R - V_A)_{max}/k_B T$  in “pure” solvents was positive (Table 1),  $10^{-3}$  M acid or base was added and the zeta potential was measured again to verify that it is weak enough. Trifluoroacetic acid (TFA) and tetrabutylammonium hydroxide (TBAH) were chosen to allow counter-ion solubility in organic solvents and avoid ionic adsorption at the particle surface. TFA was expected to increase  $\zeta$  whereas TBAH was expected to decrease  $\zeta$ . Of course, when solvents included in Table 1 already have a negative  $(V_R - V_A)_{max}/k_B T$ , the stability of dispersions was interpreted according to HSP without adding TFA or TBAH. Table 2 summarizes the experimental stabilities of the non-electrostatically stabilized dispersions which are interpreted on the basis of HSP. The solvents are listed in

Table 2 according to the increasing size of the aggregates. Each solvent is then assigned a score of 1 (stable) or 2 (unstable) based on the RTSI and the diameter of the aggregates:

Score 1:  $d_{\text{Stokes}} < 0.31 \mu\text{m}$  or  $RTSI_{2h}^{top} < 1.0$

Score 2:  $d_{\text{Stokes}} > 0.31 \mu\text{m}$  or  $RTSI_{2h}^{top} > 1.0$

Table 2 - TiO<sub>2</sub> dispersions (1 g/L) in various solvents at 25 °C for which zeta potential ( $\zeta$ ) and total interaction energy  $(V_R - V_A)_{max}$  are minimized by addition, when necessary, of 10<sup>-3</sup> M TFA (a) or TBAH (b): Relative Turbiscan Stability Index ( $RTSI_{2h}^{top}$ ), Stokes diameters ( $d_{Stokes}$ ), zeta potential ( $\zeta$ ), Hansen solvent parameters and Relative Energy Difference (RED) for the Hansen's sphere based on  $d_{Stokes}$ . Calculation details are given in SI.

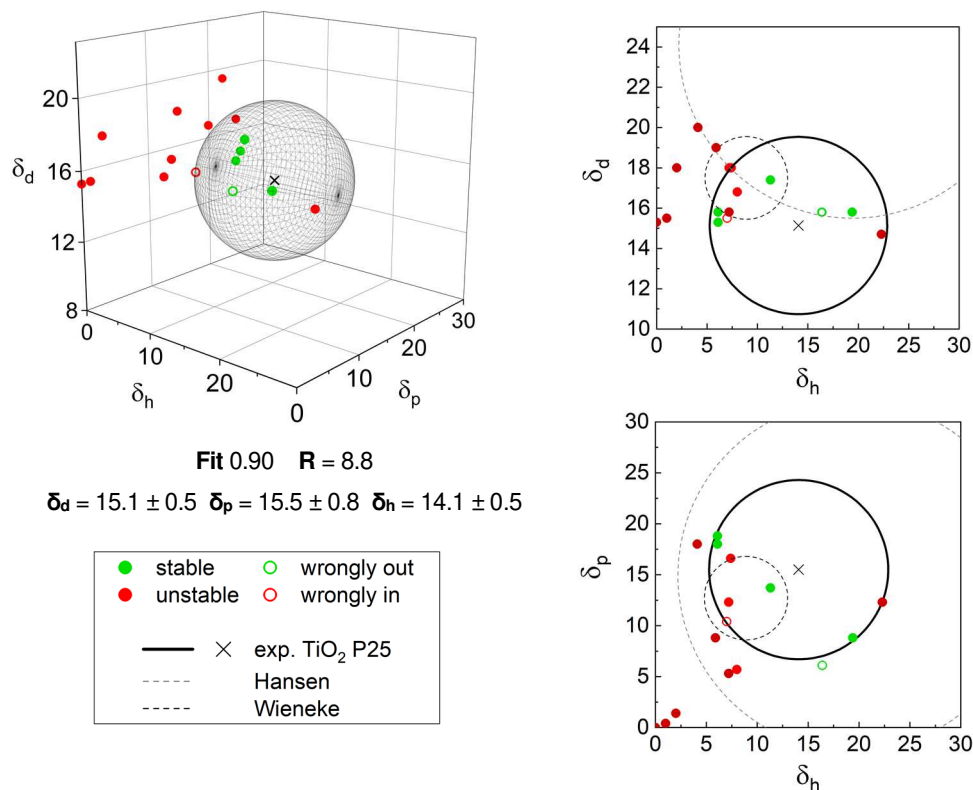
| Solvent                          | Structure   | $RTSI_{2h}^{top}$ | $d_{Stokes}$<br>( $\mu\text{m}$ ) | $\frac{(V_R - V_A)_{max}}{k_B T}$ | $\zeta$<br>(mV) | $\delta_d$ | $\delta_p$ | $\delta_h$ | RED  |
|----------------------------------|---|-------------------|-----------------------------------|-----------------------------------|-----------------|------------|------------|------------|------|
| Nitromethane <sup>a</sup>        |    | 0.30              | 0.12                              | < 0                               | -19±6           | 15.8       | 18.8       | 6.1        | 0.99 |
| Acetonitrile <sup>a</sup>        |    | 0.20              | 0.14                              | < 0                               | -11±7           | 15.3       | 18         | 6.1        | 0.95 |
| Isopropanol <sup>a</sup>         |    | 0.50              | 0.18                              | < 0                               | 15±6            | 15.8       | 6.1        | 16.4       | 1.11 |
| DMF <sup>a</sup>                 |    | 0.90              | 0.25                              | < 0                               | 12±1            | 17.4       | 13.7       | 11.3       | 0.64 |
| Ethanol <sup>b</sup>             |    | 1.00              | 0.31                              | < 0                               | -14±11          | 15.8       | 8.8        | 19.4       | 0.99 |
| NMP                              |    | 0.30              | 0.4                               | < 0                               | -7±5            | 18.0       | 12.3       | 7.2        | 1.00 |
| THF                              |  | 1.40              | 0.53                              | < 0                               | 19±2            | 16.8       | 5.7        | 8.0        | 1.36 |
| Acetone <sup>a</sup>             |  | 8.10              | 0.58                              | < 0                               | -7±4            | 15.5       | 10.4       | 7.0        | 0.99 |
| $\gamma$ -Butyrolactone          |  | 13.10             | 0.89                              | < 0                               | -4±2            | 18.0       | 16.6       | 7.4        | 1.01 |
| Propylene Carbonate <sup>a</sup> |  | 4.50              | 1.09                              | < 0                               | -18±2           | 20.0       | 18         | 4.1        | 1.61 |
| Water                            |  | 14.50             | 1.11                              | < 0                               | -5±4            | 15.5       | 16         | 42.3       | 3.21 |
| Ethyl Acetate                    |  | 2.20              | 1.14                              | < 0                               | 44±12           | 15.8       | 5.3        | 7.2        | 1.41 |
| Methanol                         |  | 10.80             | 2.88                              | < 0                               | 11±13           | 14.7       | 12.3       | 22.3       | 1.01 |
| Pyridine <sup>b</sup>            |  | 14.60             | 3.34                              | < 0                               | -24±11          | 19.0       | 8.8        | 5.9        | 1.49 |
| Heptane                          |  | 5.60              | 8.05                              | < 0                               | -10±3           | 15.3       | 0.0        | 0.0        | 2.38 |
| Toluene                          |  | 9.70              | 9.47                              | < 0                               | -30±8           | 18.0       | 1.4        | 2.0        | 2.21 |
| Triethylamine                    |  | 4.80              | 9.59                              | < 0                               | 6±6             | 15.5       | 0.4        | 1.0        | 2.27 |

<sup>a</sup> the solvent contains 10<sup>-3</sup> M trifluoroacetic acid

<sup>b</sup> the solvent contains 10<sup>-3</sup> M tetrabutylammonium hydroxide

Two HSP spheres were determined using HSPiP software considering each of the stability criteria, i.e.,  $d_{Stokes}$  or  $RTSI_{2h}^{top}$  calculated based on different methods described hereafter. The first one based on the size of the aggregates,  $d_{Stokes}$ , is shown in **Figure 8**. The “fit” indicator,

which can vary between 0 and 1, expresses the effectiveness of the sphere for modelling experimental results. The more misplaced solvents, the more the fit decreases. Here the fit is very good (0.90), since only one effective solvent (isopropanol) is excluded from the sphere and one poor solvent (acetone) is included.



**Figure 8** - HSP sphere and 2D projections of TiO<sub>2</sub> P25 1 g/L in 17 organic solvents based on Stokes diameters  $d_{\text{Stokes}}$  at 25 °C.

The second sphere calculated from  $RTSI_{2h}^{\text{top}}$  values is somewhat less satisfactory (fit = 0.88) since two effective solvents are outside the sphere and two poor solvents are inside (see Figure S 2 in SI). In both cases the radius of the sphere is 8.8 but the first sphere including all dispersions with  $d_{\text{Stokes}} < 0.31 \mu\text{m}$  appears to be the most reliable. In a study on the influence of different dispersion conditions on the size of aggregates, Jiang et al. showed that the ultrasonic probe Sonotrode provided aggregates of 155 nm [11] but was unable to further break the TiO<sub>2</sub> P25 aggregates down to the elementary particle (25 nm). In this work, we consider that particles size up to twice this minimal size provide the most stable dispersions. Beyond this size, a competition takes place between NP-solvent and NP-NP interactions that prevent the formation of smaller particles.

It is worth noting that with the first sphere (**Figure 8**), the two misplaced solvents are both located near the boundary separating effective and poor solvents. Thus, the poor solvent acetone is erroneously slightly inside the sphere with a RED of 0.99 while isopropanol

(effective solvent) is slightly outside with a RED of 1.11. RED is the “Relative Energy Difference” defined by the relationship  $RED = R_a / R$  where  $R_a$  is the distance between the solvent and the sphere centre and  $R$  is the sphere radius. So, when  $RED < 1$ , the solvent is inside the sphere and when  $RED > 1$ , the solvent is outside the sphere.

Other authors have characterized  $TiO_2$  particles [23] and nanoparticles [18] using HSP. However, none of them considered electrostatic repulsion as a possible stabilization phenomenon. Comparative results are displayed in Table 3. Characteristic parameters of the sphere calculated by Hansen regarding  $TiO_2$  pigments are very different from those determined in this study. However, Hansen investigated the paint pigment  $TiO_2$  Kronos RN 57 at a concentration 20 times greater than that of the present work [23] and no information is available regarding coating and particle diameter. Actually, it is likely that this white pigment has a diameter close to 0.3  $\mu m$  to maximize its opacifying power and that it has undergone a surface modification to avoid that the photocatalytic properties of  $TiO_2$  degrade the organic matrix of the coating. Hence, the spheres are hardly comparable.

**Table 3** - Experimentally determined Hansen parameters ( $\delta_d$ ,  $\delta_p$ ,  $\delta_h$ ), of the center and the radius ( $R$ ) of the Hansen solubility sphere and calculated Hildebrand parameter ( $\delta_H$ ) compared to literature values.

| Method                                 | $\delta_d$ [MPa <sup>1/2</sup> ] | $\delta_p$ [MPa <sup>1/2</sup> ] | $\delta_h$ [MPa <sup>1/2</sup> ] | $\delta_H$ [MPa <sup>1/2</sup> ] | R [MPa <sup>1/2</sup> ] |
|--|----------------------------------|----------------------------------|----------------------------------|----------------------------------|-------------------------|
| <b>d<sub>Stokes</sub></b>              | 15.1 ± 0.5                       | 15.5 ± 0.8                       | 14.1 ± 0.5                       | 25.8 ± 0.9                       | 8.8                     |
| <b>RTSI<sub>2h</sub><sup>top</sup></b> | 15.3 ± 0.5                       | 14.4 ± 0.6                       | 13.8 ± 0.5                       | 25.1 ± 0.8                       | 8.8                     |
| <b>Hansen [23]</b>                     | 24.1                             | 14.9                             | 19.4                             | 34.3                             | 17.2                    |
| <b>Wieneke [18]</b>                    | 17.5                             | 12.7                             | 8.9                              | 23.4                             | 4.1                     |

Differences with Wieneke’s results could come from the nature of the solvents used in both cases. Moreover, Wieneke et al. [18] studied smaller  $TiO_2$  NPs with an average particle size of 5.3 nm composed at 95 % of anatase and 5 % of rutile with a specific surface area of 265 m<sup>2</sup>/g which is much greater than that of  $TiO_2$  P25. However, the sphere obtained by Wieneke et al. is mostly included inside the one calculated in this work and the sphere radius is more than twice smaller. Also, as  $TiO_2$  NPs get smaller, interparticle forces get stronger, making dispersion harder to achieve at the expense of solvent-particle interactions [22]. Another impacting factor is the sample concentration which was of 0.015% for Wieneke’s study as the visual changes in stability are easier to detect with the naked eye in dilute samples. In their case, coagulation was evaluated through the colour change from bluish to white [18]. Using the Turbiscan, quantitative descriptors allow detecting destabilization before the naked eye could detect anything.

The Turbiscan-based method developed in this work is more reliable than those reported in

the literature to determine HSP of TiO<sub>2</sub> nanoparticles. Indeed, the phenomena occurring during the destabilization, namely the coagulation of particles and the sedimentation of aggregates, can be observed separately. Moreover, this work clearly shows that, when particles are charged and dispersed in polar solvents, the electrostatic repulsion must absolutely be taken into account to rationalize the observed stabilities using DLVO theory. As electrostatic repulsions are not considered in Hansen's theory, only dispersions of weakly charged particles in media of low polarity can correctly be interpreted on the basis of HSP. Therefore, it makes no sense to interpret the stability of DLVO stabilized samples using HSP theory. On the other hand, the analysis of the stability of the dispersions jointly by Hansen's and DLVO theories provides complementary information allowing a more accurate interpretation of the results and highlight the solvents exhibiting a significant affinity for the particles' surface.

#### 4. Conclusion

Hansen Solubility Parameters (HSP) have been used for rationalizing and predicting the stability of titanium dioxide particles dispersions [13,18,23]. However, interparticle electrostatic interactions, not considered in Hansen's approach but considered in the DLVO theory, play a significant role in organic solvents having a notable dielectric constant [15,56,57]. HSP interpretation for NPs dispersions can be achieved provided that electrostatic repulsion is accounted for, in particular regarding inorganic NPs that can easily acquire surface charges.

In water, it was shown that the Turbiscan detected high *TSI* (Turbiscan Stability Index) and Stokes diameters when zeta potential was elevated, in accordance with the DLVO theory. In organic solvents, it was intended to interpret the stability using HSP. This model was shown insufficient to describe with fidelity the dispersions stability since no sphere could fit the experimental observations. The relevance of DLVO interpretation came in to play as total repulsive energy  $(V_R - V_A)_{max}$  was non-negligible in numerous solvents. When the zeta potential of NPs and the dielectric constant of the solvent are both high, the dispersion benefits from additional stabilization while when the electrostatic repulsion is negligible, only the solvents within a Hansen dispersion sphere give stable dispersions. The two interpretations are therefore complementary to describe the behavior of TiO<sub>2</sub> dispersions in organic solvents.

Using a zeta dip cell, with higher chemical compatibility than the regular folded capillary cells, it was possible to measure zeta potential in organic solvents and assess the strength of the electrostatic contribution to stabilization. Solvents were scored according to Turbiscan indicators, namely  $RTSI_{2h}^{top}$  (Relative Turbiscan Stability Index after 2 hours at the top of the

cell) and  $d_{\text{Stokes}}$  calculated from the sedimentation rate to yield the TiO<sub>2</sub> P25 Hansen Solubility Sphere. The sphere ( $R = 8.8$ ,  $\delta_d = 15.1$ ,  $\delta_p = 15.5$ ,  $\delta_h = 14.1 \text{ MPa}^{1/2}$ ) was compared to that of Hansen [23] and that of Wieneke et al. [18] for TiO<sub>2</sub>, both determined based on visual scoring. In this study, both zeta measurement and Turbiscan monitoring of stability were complementary.  $RTSI_{2h}^{top}$  and Stokes diameters are quantitative descriptors avoiding an empirical visual rating of dispersions stability. Future HSP

determination for other types of NPs such as metal oxides or carbon-based NPs should validate this method.

### Acknowledgements

We gratefully acknowledge the Chevreul Institute (FR 2638), the Ministère de l'Enseignement Supérieur et de la Recherche, the Région Hauts-de-France, the MEL (Métropole Européenne de Lille) and the Université de Lille for their financial support. We also thank Jordan Bassetti, Mehdi Hanot and Mike Ortega Vaz for their technical assistance and contribution to obtaining sedimentation scans.

### References

- [1] Commission recommendation of 18 October 2011 on the definition of nanomaterial text with EEA relevance, 2011. <http://data.europa.eu/eli/reco/2011/696/oj/eng> (accessed April 3, 2020).
- [2] R.C. Monica, R. Cremonini, Nanoparticles and higher plants, *Caryologia*. 62 (2009) 161–165. <https://doi.org/10.1080/00087114.2004.10589681>.
- [3] G.M. Whitesides, Nanoscience, nanotechnology, and chemistry, *Small*. 1 (2005) 172–179. <https://doi.org/10.1002/sml.200400130>.
- [4] S.L. Schneider, H.W. Lim, A review of inorganic UV filters zinc oxide and titanium dioxide, *Photodermatol Photoimmunol Photomed*. 35 (2019) 442–446. <https://doi.org/10.1111/phpp.12439>.
- [5] S. Yashwant Singh, Nano titanium dioxide market by application (paints & coatings, pigments, cosmetics, plastics, energy and others) - Global opportunity analysis and industry forecast, 2014 - 2022, 2016. <https://www.alliedmarketresearch.com/nano-titanium-dioxide-market> (accessed April 6, 2020).
- [6] J. Papp, S. Soled, K. Dwight, A. Wold, Surface acidity and photocatalytic activity of TiO<sub>2</sub>, WO<sub>3</sub>/TiO<sub>2</sub>, and MoO<sub>3</sub>/TiO<sub>2</sub> photocatalysts, *Chem. Mater*. 6 (1994) 496–500. <https://doi.org/10.1021/cm00040a026>.
- [7] S. Pilotek, K. Gossmann, F. Tabellion, K. Steingröver, H. Homann, Tailored nanoscaled TiO<sub>2</sub> dispersions for photocatalytic applications, in: Technical proceedings of the 2009 clean technology conference and trade show, Houston, USA, 2009: pp. 304–307.
- [8] Product information AEROXIDE® TiO<sub>2</sub> P25, (2019). <https://products-re.evonik.com/www2/uploads/productfinder/AEROXIDE-TiO2-P-25-EN.pdf> (accessed March 24, 2020).
- [9] J. Schulz, H. Hohenberg, F. Pflücker, E. Gärtner, T. Will, S. Pfeiffer, R. Wepf, V. Wendel, H. Gers-Barlag, K.-P. Wittern, Distribution of sunscreens on skin, *Adv. Drug Deliv. Rev*. 54 (2002) S157–S163. [https://doi.org/10.1016/S0169-409X\(02\)00120-5](https://doi.org/10.1016/S0169-409X(02)00120-5).

- [10] G. Li, L. Lv, H. Fan, J. Ma, Y. Li, Y. Wan, X.S. Zhao, Effect of the agglomeration of TiO<sub>2</sub> nanoparticles on their photocatalytic performance in the aqueous phase, *J. Colloid Interface Sci.* 348 (2010) 342–347. <https://doi.org/10.1016/j.jcis.2010.04.045>.
- [11] J. Jiang, G. Oberdörster, P. Biswas, Characterization of size, surface charge, and agglomeration state of nanoparticle dispersions for toxicological studies, *J Nanopart Res.* 11 (2009) 77–89. <https://doi.org/10.1007/s11051-008-9446-4>.
- [12] J. Qin, X. Wang, Q. Jiang, M. Cao, Optimizing dispersion, exfoliation, synthesis, and device fabrication of inorganic nanomaterials using Hansen solubility parameters, *ChemPhysChem.* 20 (2019) 1069–1097. <https://doi.org/10.1002/cphc.201900110>.
- [13] S. Süß, T. Sobisch, W. Peukert, D. Lerche, D. Segets, Determination of Hansen parameters for particles: a standardized routine based on analytical centrifugation, *Adv Powder Technol.* 29 (2018) 1550–1561. <https://doi.org/10.1016/j.apt.2018.03.018>.
- [14] H. Buron, O. Mengual, G. Meunier, I. Cayré, P. Snabre, Optical characterization of concentrated dispersions: applications to laboratory analyses and on-line process monitoring and control, *Polym Int.* 53 (2004) 1205–1209. <https://doi.org/10.1002/pi.1231>.
- [15] S.H. Woo, L. Min Gu, C.K. Rhee, Sedimentation properties of TiO<sub>2</sub> nanoparticles in organic solvents, *Solid State Phenom.* 119 (2007) 267–270. <https://doi.org/10.4028/www.scientific.net/SSP.119.267>.
- [16] Z.Q. Liu, X. Yang, Q. Zhang, Turbiscan: history, development, application to colloids and dispersions, *Adv Mat Res.* 936 (2014) 1592–1596. <https://doi.org/10.4028/www.scientific.net/AMR.936.1592>.
- [17] M. Luo, X. Qi, T. Ren, Y. Huang, A.A. Keller, H. Wang, B. Wu, H. Jin, F. Li, Heteroaggregation of CeO<sub>2</sub> and TiO<sub>2</sub> engineered nanoparticles in the aqueous phase: application of turbiscan stability index and fluorescence excitation-emission matrix (EEM) spectra, *Colloids Surf. A.* 533 (2017) 9–19. <https://doi.org/10.1016/j.colsurfa.2017.08.014>.
- [18] J.U. Wieneke, B. Kommoß, O. Gaer, I. Prykhodko, M. Ulbricht, Systematic investigation of dispersions of unmodified inorganic nanoparticles in organic solvents with focus on the Hansen solubility parameters, *Ind. Eng. Chem. Res.* 51 (2012) 327–334. <https://doi.org/10.1021/ie201973u>.
- [19] S. Kuchler, T. Detloff, T. Sobisch, D. Lerche, Direct and accelerated characterization of ceramic dispersions, *Ceramic Forum International. cfi/Ber. DKG 88* (2011) (2011) E27–E31.
- [20] L. Xu, H.-W. Liang, Y. Yang, S.-H. Yu, Stability and reactivity: positive and negative aspects for nanoparticle processing, *Chem. Rev.* 118 (2018) 3209–3250. <https://doi.org/10.1021/acs.chemrev.7b00208>.
- [21] J.N. Israelachvili, Intermolecular and surface forces, Revised third edition, Academic Press, 2011.
- [22] M. Hosokawa, K. Nogi, M. Naito, T. Yokoyama, Nanoparticle technology handbook, Second edition, Elsevier, Amsterdam, 2012.
- [23] C.M. Hansen, The three dimensional solubility parameter and solvent diffusion coefficient, Danish Technical Press, Copenhagen, 1967. <https://hansen-solubility.com/contents/HSP1967-OCR.pdf> (accessed March 9, 2020).
- [24] C. Hansen, S. Abbott, H. Yamamoto, HSP Examples: Nanoparticles | Hansen Solubility Parameters, (2020). <https://www.hansen-solubility.com/HSP-examples/nanoparticles.php> (accessed April 9, 2020).
- [25] L.M. Wheeler, N.J. Kramer, U.R. Kortshagen, Thermodynamic driving force in the spontaneous formation of inorganic nanoparticle solutions, *Nano Lett.* 18 (2018) 1888–1895. <https://doi.org/10.1021/acs.nanolett.7b05187>.
- [26] C. Stauch, S. Süß, R. Luxenhofer, B.P. Binks, D. Segets, K. Mandel, Quantifying surface properties of silica particles by combining Hansen parameters and Reichardt's dye indicator data, *Part. Part. Syst. Charact.* 35 (2018) 1800328. <https://doi.org/10.1002/ppsc.201800328>.



- [27] H. Launay, C.M. Hansen, K. Almdal, Hansen solubility parameters for a carbon fiber/epoxy composite, *Carbon*. 45 (2007) 2859–2865. <https://doi.org/10.1016/j.carbon.2007.10.011>.
- [28] C.M. Hansen, A.L. Smith, Using Hansen solubility parameters to correlate solubility of C60 fullerene in organic solvents and in polymers, *Carbon*. 42 (2004) 1591–1597. <https://doi.org/10.1016/j.carbon.2004.02.011>.
- [29] Y. Hernandez, M. Lotya, D. Rickard, S.D. Bergin, J.N. Coleman, Measurement of multicomponent solubility parameters for graphene facilitates solvent discovery, *Langmuir*. 26 (2010) 3208–3213. <https://doi.org/10.1021/la903188a>.
- [30] H.T. Ham, Y.S. Choi, I.J. Chung, An explanation of dispersion states of single-walled carbon nanotubes in solvents and aqueous surfactant solutions using solubility parameters, *J. Colloid Interface Sci.* 286 (2005) 216–223. <https://doi.org/10.1016/j.jcis.2005.01.002>.
- [31] K. Maleski, V.N. Mochalin, Y. Gogotsi, Dispersions of two-dimensional titanium carbide MXene in organic solvents, *Chem. Mater.* 29 (2017) 1632–1640. <https://doi.org/10.1021/acs.chemmater.6b04830>.
- [32] S. Mathioudaki, B. Barthélémy, S. Detriche, C. Vandenberghe, J. Delhalle, Z. Mekhalif, S. Lucas, Plasma treatment of metal oxide nanoparticles: development of core–shell structures for a better and similar dispersibility, *ACS Appl. Nano Mater.* 1 (2018) 3464–3473. <https://doi.org/10.1021/acsanm.8b00645>.
- [33] AEROXIDE®, AERODISP® and AEROPERL® titanium dioxide as photocatalyst - Technical information 1243, (2015). <https://www.aerosil.com/sites/lists/RE/DocumentsSI/TI-1243-Titanium-Dioxide-as-Photocatalyst-EN.pdf> (accessed April 3, 2020).
- [34] Technical overview 13 - AEROXIDE® - Fumed metal oxides, (2017). <https://www.aerosil.com/product/aerosil/downloads/to-aeroxide-en.pdf> (accessed March 24, 2020).
- [35] Application note TS\_STAB\_60 Explanation to the TSI calculation, (2019).
- [36] P. Mills, P. Snabre, Settling of a suspension of hard spheres, *EPL*. 25 (1994) 651. <https://doi.org/10.1209/0295-5075/25/9/003>.
- [37] Application note - Zeta potential measurements of non-aqueous particulate suspensions, (2010).
- [38] I.M. Tucker, J.C.W. Corbett, J. Fatkin, R.O. Jack, M. Kaszuba, B. MacCreath, F. McNeil-Watson, Laser Doppler Electrophoresis applied to colloids and surfaces, *Curr Opin Colloid Interface Sci.* 20 (2015) 215–226. <https://doi.org/10.1016/j.cocis.2015.07.001>.
- [39] I.D. Morrison, S. Ross, *Colloidal dispersions: suspensions, emulsions, and foams*, Wiley, 2002.
- [40] R.J. Hunter, *Zeta potential in colloid science: principles and applications*, Academic Press, New York, 1981.
- [41] M. Kosmulski, Zeta potentials in nonaqueous media: how to measure and control them, *Colloids Surf. A*. 159 (1999) 277–281. [https://doi.org/10.1016/S0927-7757\(99\)00273-3](https://doi.org/10.1016/S0927-7757(99)00273-3).
- [42] M. Kosmulski, P. Eriksson, J.B. Rosenholm, Application of zetametry to determine concentrations of acidic and basic impurities in analytical reagents, *Anal. Chem.* 71 (1999) 2518–2522. <https://doi.org/10.1021/ac9806052>.
- [43] M. Kosmulski, *Surface charging and points of zero charge*, CRC Press, 2009. <https://doi.org/10.1201/9781420051896>.
- [44] K. Bourikas, T. Hiemstra, W.H. Van Riemsdijk, Ion pair formation and primary charging behavior of titanium oxide (anatase and rutile), *Langmuir*. 17 (2001) 749–756. <https://doi.org/10.1021/la000806c>.
- [45] A. Foissy, A. M'Pandou, J.M. Lamarche, N. Jaffrezic-Renault, Surface and diffuse-layer charge at the TiO<sub>2</sub>-electrolyte interface, *Colloids Surf.* 5 (1982) 363–368. [https://doi.org/10.1016/0166-6622\(82\)80046-2](https://doi.org/10.1016/0166-6622(82)80046-2).

- [46] B. Derjaguin, L. Landau, Theory of the stability of strongly charged lyophobic sols and of the adhesion of strongly charged particles in solutions of electrolytes, *Acta Physicochim. U.R.S.S.* 14 (1941) 633–662.
- [47] E.J.W. Verwey, J.T.G. Overbeek, K. van Nes, Theory of the stability of lyophobic colloids: the interaction of sol particles having an electric double layer, Elsevier Publishing Company, Amsterdam, 1948.
- [48] K. Suttiponpannit, J. Jiang, M. Sahu, S. Suvachittanont, T. Charinpanitkul, P. Biswas, Role of surface area, primary particle size, and crystal phase on titanium dioxide nanoparticle dispersion properties, *Nanoscale Res Lett.* 6 (2010) 27. <https://doi.org/10.1007/s11671-010-9772-1>.
- [49] J. Qi, Y.Y. Ye, J.J. Wu, H.T. Wang, F.T. Li, Dispersion and stability of titanium dioxide nanoparticles in aqueous suspension: effects of ultrasonication and concentration, *Water Science and Technology.* 67 (2013) 147–151. <https://doi.org/10.2166/wst.2012.545>.
- [50] R. Beranek, (Photo)electrochemical methods for the determination of the band edge positions of TiO<sub>2</sub>-based nanomaterials, *Adv. Phys. Chem.* (2011). <https://doi.org/10.1155/2011/786759>.
- [51] M. Herrmann, H.P. Boehm, Über die Chemie der Oberfläche des Titandioxids. ii. Saure Hydroxylgruppen auf der Oberfläche, *Z Anorg Allg Chem.* 368 (1969) 73–86. <https://doi.org/10.1002/zaac.19693680111>.
- [52] M.A. Butler, D.S. Ginley, Prediction of flatband potentials at semiconductor-electrolyte interfaces from atomic electronegativities, *J. Electrochem. Soc.* 125 (1978) 228. <https://doi.org/10.1149/1.2131419>.
- [53] C. Kormann, D.W. Bahnemann, M.R. Hoffmann, Photolysis of chloroform and other organic molecules in aqueous titanium dioxide suspensions, *Environ. Sci. Technol.* 25 (1991) 494–500. <https://doi.org/10.1021/es00015a018>.
- [54] J. Lyklema, Principles of the stability of lyophobic colloidal dispersions in non-aqueous media, *Adv. Colloid Interface Sci.* 2 (1968) 67–114. [https://doi.org/10.1016/0001-8686\(68\)85001-8](https://doi.org/10.1016/0001-8686(68)85001-8).
- [55] R. Hogg, T.W. Healy, D.W. Fuerstenau, Mutual coagulation of colloidal dispersions, *Trans. Faraday Soc.* 62 (1966) 1638–1651. <https://doi.org/10.1039/TF9666201638>.
- [56] J.B. Rosenholm, P. Dahlsten, Influence of charge exchange in acidic aqueous and alcoholic titania dispersions on viscosity, *Advances in Colloid and Interface Science.* 226 (2015) 138–165. <https://doi.org/10.1016/j.cis.2015.10.007>.
- [57] N.D. Burrows, E. Kesselman, K. Sabyrov, A. Stemig, Y. Talmon, R. Lee Penn, Crystalline nanoparticle aggregation in non-aqueous solvents, *CrystEngComm.* 16 (2014) 1472–1481. <https://doi.org/10.1039/C3CE41584H>.
- [58] K. Izutsu, Acid–base reactions in nonaqueous solvents, in: *Electrochemistry in nonaqueous solutions*, John Wiley & Sons, Ltd, 2009: pp. 63–87. <https://doi.org/10.1002/9783527629152.ch3>.
- [59] J. Barbosa, C.M. Bosch, V. Sanz-Nebot, Effect of the solvent on the equilibria of acid-base indicators in aprotic and amphiprotic solvents, *Mikrochim. Acta.* 106 (1992) 327–337. <https://doi.org/10.1007/BF01242105>.
- [60] O. Popovych, Transfer activity coefficients of ions in methanol-water solvents based on the tetraphenylborate assumption, *J. Phys. Chem.* 88 (1984) 4167–4170. <https://doi.org/10.1021/j150662a063>.
- [61] M. Kosmulski, E. Matijević, Zeta potential of anatase (TiO<sub>2</sub>) in mixed solvents, *Colloids Surf.* 64 (1992) 57–65. [https://doi.org/10.1016/0166-6622\(92\)80162-U](https://doi.org/10.1016/0166-6622(92)80162-U).
- [62] W. Janusz, A. Sworska, J. Szczypa, The structure of the electrical double layer at the titanium dioxide/ethanol solutions interface, *Colloids Surf. A.* 152 (1999) 223–233. [https://doi.org/10.1016/S0927-7757\(98\)00341-0](https://doi.org/10.1016/S0927-7757(98)00341-0).
- [63] S.H. Behrens, D.I. Christl, R. Emmerzael, P. Schurtenberger, M. Borkovec, Charging and aggregation properties of carboxyl latex particles: experiments versus DLVO theory, *Langmuir.* 16 (2000) 2566–2575. <https://doi.org/10.1021/la991154z>.

- [64] E. Hückel, P. Debye, Zur Theorie der Elektrolyte. I. Gefrierpunktserniedrigung und verwandte Erscheinungen, *Phys. Z.* 24 (1923) 185–206.
- [65] H.C. Hamaker, The London-van der Waals attraction between spherical particles, *Physica.* 4 (1937) 1058–1072. [https://doi.org/10.1016/S0031-8914\(37\)80203-7](https://doi.org/10.1016/S0031-8914(37)80203-7).
- [66] T. Tadros, Chapter 2 - Colloid and interface aspects of pharmaceutical science, in: H. Ohshima, K. Makino (Eds.), *Colloid and interface science in pharmaceutical research and development*, Elsevier, Amsterdam, 2014: pp. 29–54. <https://doi.org/10.1016/B978-0-444-62614-1.00002-8>.